Volume XXIX 2026
MBNA Publishing House Constanta 2026

Scientific Bulletin of Naval Academy

SBNA PAPER • OPEN ACCESS

Modeling and optimization of battery-based energy storage systems for UAVs

To cite this article: Pascu Adrian-Nicolae, Popa Nicolae-Silviu1, Cristea Ovidiu, Deliu Florențiu and Șerban Ionuț, Scientific Bulletin of Naval Academy, Vol. XXIX 2026, pg. 176-193.

Submitted: 21.04.2026
Revised: 31.07.2026
Accepted: 04.08.2026

Available online at www.anmb.ro

ISSN: 2392-8956; ISSN-L: 1454-864X

doi: 10.21279/1454-864X-26-I1-017

Modeling and optimization of battery-based energy storage systems for UAVs

Pascu Adrian-Nicolae[1], Popa Nicolae-Silviu[1*], Cristea Ovidiu[1], Deliu Florențiu[1], Șerban Ionuț[2]

1 Romanian Naval Academy 'Mircea cel Batran', Fulgerului Street, no.1, Constanta
2 Maritime Hydrographic Directorate 'Commander Alexandru Cătuneanu', Fulgerului Street, no.1, Constanta
Popa Nicolae-Silviu – silviu.popa@anmb.ro

Abstract. The paper presents the improvement of the energy efficiency of drones used in different missions. In this paper, a model for Li-ion batteries is created, made through equivalent electrical circuits. This method facilitates the examination of the relationship between the required energy consumption and the electrical response of the battery to demands.
The results were introduced into MATLAB, where a model of Li-Ion batteries was created based on equivalent circuits, which facilitated the examination of energy consumption during the mission and the demands to which the battery is exposed in different flight regimes. The obtained results facilitate us to show the efficiency of hybrid batteries. The integration of the supercapacitor facilitates the performance of the battery battery, resulting in superior voltage stability but also increased resistance to different operating regimes.
In conclusion, the paper aims at numerical modeling, simulation, development and optimization of energy architectures for UAV systems.
Keywords: UAV flight endurance optimization, MATLAB-based simulation, research unmanned aerial vehicles, energy storage systems, lithium-ion batteries.

1. Introduction

The use of aerial vehicles in various marine applications—such as monitoring, mapping, research, and surveillance—has grown rapidly. Their operational range is a decisive factor that can influence their performance and efficiency.

Energy storage systems are essential for drone operation; most drones utilize Li-Ion batteries due to their energy efficiency. However, these batteries are affected by changing operating conditions, which can accelerate their deterioration and lead to performance degradation.In this sense, hybrid systems for electronic management, which include capacitor batteries, represent a new innovative solution with a much higher efficiency.

The use of these technologies leads to efficient power distribution but also to reduced battery degradation. This article analyzes the optimization and management of drone energy systems by using electro-thermal modeling and numerical simulation in MATLAB, considering the optimization of architectural performance and the impact it has on flight autonomy.

2. Surface platforms / USV-type drones

The first USV drone was designed and developed within an MIT Sea Grant College program in the 1990s, being inspired by future production, resulting in a multitude of USV models, for carrying out different types of operations. The maritime industry is the basis for the development of USV drones, and their use allows for the carrying out of different types of missions in the marine environment, both military and civilian.[1]

2.1. Applications of Drones in the Maritime Sector

In the marine environment, the use of drones to perform various high-risk missions has led to the development of a multitude of roles that they can perform. Their use considerably reduces the risks to which human personnel may be subjected, the costs, but also the duration of the mission.[1], [2]

Some of the applications of drones in the marine environment are mentioned below:

- Routine inspections of: ship hull, ballast tanks, structural integrity, etc.;
- Mooring facility inspections;
- Damage detection surveys.

Drones are equipped and adapted to carry out missions in hard-to-reach areas and transmit information to the persons designated to carry out the mission. Their use in the marine environment includes activities such as:

- Support of operations in the high seas and ports;
- Search and rescue;
- Delivery of warning systems;
- Detection of objects at sea;
- Delivery of goods, documents and medicines to ships at sea;
- Prevention of illegal migration in customs areas;
- Monitoring of ports;
- Detection of activities in the high seas such as illegal fishing or drug trafficking;
- Pollution monitoring.

2.2. Propulsion System of USV Drones

Current drone propulsion systems use either a hybrid or electric propulsion system.
A hybrid system uses a combination of energy sources such as diesel generators, batteries, or fossil fuels. However, this type of propulsion uses the heat from the engine and fossil fuels along with the energy stored in the batteries. [3]Hybrid electric vehicles convert energy into electricity when the diesel generator produces more power than is needed to propel the device. A key feature of hybrid electric platforms is their ability to sequester excess energy; when the diesel generator's output exceeds the immediate propulsion demand, the surplus is converted and stored as electrical power for later use.

Conversely, the pure electric propulsion framework is bifurcated into two primary subsystems: power generation and flight control. The former incorporates a dedicated wireless emergency cutoff mechanism alongside a dual 24V battery configuration. To ensure operational redundancy and minimize electrical interference, these power sources are isolated: one battery is dedicated exclusively to driving the dual-thruster assembly, while the second unit provides a stable voltage supply for the drone's command and control electronics.[4]

3. Battery Technologies for Energy Storage

The operational logic of modern batteries is rooted in the electrochemical dynamics of energy storage. These systems rely on redox reactions, where the migration of electrons between electrodes facilitates the conversion of potential chemical energy into electrical power. Based on the specific chemistry of the internal cells, these storage units are categorized across several distinct technologies:[5]

- Carbon-Zinc Batteries: Traditionally yielding a nominal 1.5 V, these cells suffer from a progressive voltage drop during discharge. Furthermore, their electrochemical efficiency is severely compromised in sub-zero thermal environments.
- Alkaline Batteries: Developed as a high-performance successor to carbon-zinc chemistries, alkaline cells offer a fivefold increase in energy output and superior energy density. While they exhibit enhanced cycle stability and improved functional efficiency, their primary drawback remains their primary (non-rechargeable) nature.
- Nickel-Cadmium (Ni-Cd) Batteries: Capable of roughly 1,000 recharge cycles, these units maintain a stable 1.2–1.5 V output even under harsh environmental stress. Although they provide a longer service life and lower maintenance overhead than lithium-based alternatives, they are hindered by lower specific energy and higher manufacturing costs. Moreover, the high toxicity of cadmium necessitates rigorous hazardous waste protocols at the end of their lifecycle.[6]
- Li-Ion batteries are is based on electrochemical redox reactions, in which lithium ions intercalate into the crystal structure of the electrode materials.[6]

4. Mathematical Modeling of the Energy Storage System

In the context of drones used in research, the energy storage mechanism is a critical component to guarantee the device's ability to operate autonomously, in a stable and safe regime.[7] As a result, battery modeling, especially lithium-ion batteries, transcends the simple estimation of energy capacity, becoming essential for optimizing resource planning and mission coordination.

Given the restrictive nature of UAV platforms, limited by their low mass, modest processing resources and the need for immediate operability, it is necessary to develop models that achieve an optimal compromise between data accuracy and the computational effort required.[7], [8]

The hierarchy of battery models can be achieved at various levels, depending on the level of detail of the analyzed phenomena. [9]Although electrochemical models faithfully reproduce the internal mechanisms, their high mathematical complexity makes them difficult to implement in integrated architectures. A more accessible alternative is empirical models, which use equivalent electrical circuits to describe their behavior.

4.1. Macro-Homogeneous Electrochemical Model (Pseudo-2D)

The macro-homogeneous electrochemical model, known as the Pseudo-2D (P2D) model, based on the theory developed by John Newman, is one of the most advanced approaches to describe the behavior of Lithium-Ion batteries.[10] This model provides a detailed representation of species transport phenomena and electrochemical reaction kinetics at the microscopic scale, and is considered a reference standard in the specialized literature.

The transport of lithium in the solid phase is described by the diffusion equation derived from Fick's second law, formulated in spherical coordinates for the active particles of the electrodes.

This equation governs the evolution of lithium concentration and imposes direct constraints on the maximum charge and discharge rates—critical considerations for drones performing maneuvers that require high power. Mathematically, the relation is expressed as follows:[11]

$$\frac{\partial c_{s,i}}{\partial t} = \frac{1}{r^2}\frac{\partial}{\partial r}(D_{s,i} r^2 \frac{\partial c_{s,i}}{\partial r})$$

Where:

- $c_{s,i}$ represents the lithium concentration in the solid phase;
- $D_{s,i}$ is the diffusion coefficient in the active material of electrode i;
- r is the radial coordinate of the particle.

4.2. Equivalent Electrical Circuit (EEC) Modeling

In the case of the first-order RC model, the voltage at the battery terminals is expressed as the sum of the contributions from the electromotive force, the instantaneous ohmic losses and the transient effects associated with diffusion processes, modeled by a resistive-capacitive branch. The discrete equation of the voltage at the terminals is given by the relation:[12]

$$v[k] = OCV(z[k]) + M \cdot h[k] - R_1 \cdot i_{R1}[k] - R_0 \cdot i[k]$$

Where:

- $OCV(z[k])$ represents the open-circuit voltage (electromotive force), dependent on the battery state of charge $z[k]$, determined thermodynamically according to Nernst's relation.
- $M \cdot h[k]$ is the hysteresis term, introduced to model voltage differences between charge and discharge regimes.
- $R_1 \cdot i_{R1}[k]$ defines the polarization voltage, associated with slow transient phenomena and internal diffusion processes.
- $R_0 \cdot i[k]$ represents the ohmic voltage drop, determined by the series resistance of the battery R_0, proportional to the instantaneous current $i[k]$, corresponding to energy losses through Joule heating.

4.3. State of Charge (SOC) Modeling

The fundamental method for estimating SOC is the Coulomb counting technique, which is based on the integration of current over time and reflects the evolution of the charge stored in the battery. The mathematical definition of SOC is expressed as:[6], [13]

$$z(t) = z(t_0) - \frac{1}{Q_{\text{tot}}} \int_{t_0}^{t} \eta \, i(\tau) \, d\tau$$

Where:

- $z(t)$ represents the state of charge (SOC) at the current time t;
- $z(t_0)$ is the initial SOC at the reference time t_0;
- Q_{tot} is the total battery capacity, expressed in Coulombs;
- η is the Coulombic efficiency of the battery, which for Li-Ion batteries is approximately equal to 1;
- $i(\tau)$ is the instantaneous current as a function of time, considered positive during discharge.

4.4. Thermal Behavior Modeling

During UAV operation, the high-power demands of the propulsion system lead to large currents through the battery, generating heat both through Joule effects and internal electrochemical processes. Temperature directly influences battery performance, degradation rate and operational safety, which is why thermal behavior modeling is indispensable in storage system analysis.[14]

At a general level, the temperature distribution is described by the energy conservation equation, which takes into account thermal conduction and internal heat generation:[15]

$$\rho C_p \frac{\partial T}{\partial t} = \nabla \cdot (\lambda \nabla T) + q_{\text{irr}} + q_{\text{rev}} + q_{\text{ohm}}$$

Where:

- ρ is the material density;
- C_p is the specific heat capacity of the material;
- λ is the thermal conductivity;
- T is the temperature;
- q_{irr} represents irreversible heat, associated with activation losses of electrochemical reactions;
- q_{rev} is reversible (entropic) heat, determined by entropy changes during lithium intercalation processes;
- q_{ohm} corresponds to Joule heat generated by internal battery resistances and electrical conduction processes in the electrodes and electrolyte.

4.5. Battery Degradation and State of Health (SOH) Modeling

Battery health represents its operating capacity in conjunction with initial performance and is an indicator for the long-term operation of drones.[15], [16]

The technical degradation of Li-Ion batteries is a process that encompasses temperature, high currents, and repetitive charging.

Formally, SOH can be defined based on capacity loss as:

$$SOH_Q = \frac{Q_{\text{actual}}}{Q_{\text{nominal}}} \times 100\%$$

Where:

- Q_{actual} is the available battery capacity at a given time;
- Q_{nominal} is the initial (nominal) battery capacity.

A complementary approach models degradation through internal resistance growth, using a semi-empirical model:

$$R_{\text{life}} = a_0 + a_1 t^{\frac{1}{2}} + a_2 N$$

Where:

- a_0 represents the initial battery resistance;
- $a_1 t^{1/2}$ describes the increase in internal resistance associated with slow, diffusion-limited processes, such as SEI layer formation;
- $a_2 N$ reflects degradation induced by repeated operational cycles, where N is the number of flight cycles.

These models allow for the estimation of battery lifetime and support predictive maintenance strategies for UAV fleets.

5. Numerical Analysis and Optimization of the Hybrid Energy Storage System for UAVs in MATLAB

The model allows for the simultaneous investigation of charging, voltage, discharge current, power distribution and thermal behavior of the system. By using nonlinear optimization, the optimal battery mass for energy efficiency can be determined, taking into account the dependence between the drone mass and power consumption.

5.1. Simulation Environment Initialization

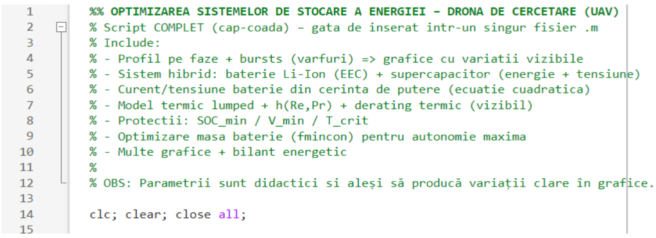

```
%% OPTIMIZAREA SISTEMELOR DE STOCARE A ENERGIEI - DRONA DE CERCETARE (UAV)
% Script COMPLET (cap-coada) - gata de inserat intr-un singur fisier .m
% Include:
% - Profil pe faze + bursts (varfuri) => grafice cu variatii vizibile
% - Sistem hibrid: baterie Li-Ion (EEC) + supercapacitor (energie + tensiune)
% - Curent/tensiune baterie din cerinta de putere (ecuatie cuadratica)
% - Model termic lumped + h(Re,Pr) + derating termic (vizibil)
% - Protectii: SOC_min / V_min / T_crit
% - Optimizare masa baterie (fmincon) pentru autonomie maxima
% - Multe grafice + bilant energetic
%
% OBS: Parametrii sunt didactici si aleși să producă variații clare în grafice.

clc; clear; close all;
```

Figure 1: Energy Storage System Optimization

Initialization serves to eliminate residual states (variables, figures, and outputs from previous sessions) that could affect the reproducibility of results. In the context of numerical simulations for energy systems, reproducibility is essential, as parameters are often calibrated based on specific datasets, and the comparability of scenarios (standard vs. optimized) must be strictly maintained.

5.2. Definition of Physical Constants and Air Properties

```
%% 1) CONSTANTE FIZICE SI AER
g        = 9.81;       % [m/s^2]
rho_air  = 1.225;      % [kg/m^3]
k_air    = 0.026;      % [W/m/K]
nu_air   = 1.5e-5;     % [m^2/s]
Pr_air   = 0.71;       % [-]

```

Figure 2: Physical Constants and Air Properties

Figure 2 shows the external environment parameters, which are necessary for aerodynamic efficiency, as well as the thermal model. The parameters k_air, ν_air and Pr also intervene to estimate the coefficient h through the Nusselt number, specific to the following equation:[17]

$$Nu = \frac{hL}{k_{\text{air}}}, Re = \frac{vL}{\nu_{\text{air}}}, Nu \sim Re^{\frac{1}{2}} Pr^{\frac{1}{3}}.$$

In this way, battery cooling becomes dependent on the flight regime (air velocity), which provides the model with enhanced physical consistency.

5.3. Parameterization of the UAV Platform and Auxiliary Loads

```
%% 2) DATE DRONA
masa_structura     = 2.4;      % [kg]
masa_maxima        = 4.0;      % [kg]
A_disk             = 0.05;     % [m^2]
eta_motor          = 0.87;     % [-]
P_electronica      = 22;       % [W]
P_senzori          = 18;       % [W]
CdA                = 0.03;     % [m^2] (simplificat)

```

Figure 3: UAV Data

The model separates the structural mass (fixed component) from the energy system mass (variable component). This distinction is important because the battery mass simultaneously affects the available energy and mechanical consumption (through the increase in induced power).

Electronic and sensor loads are introduced as a constant term, representing "parasitic loads" that must be sustained regardless of the aerodynamic regime. The parameter $C_d A$consolidates the effects of aerodynamic drag into a scalar formulation, which is subsequently used in the calculation of propulsion power.

5.4. Definition of the Li-Ion Battery Model (Electrical Parameters and OCV)

```
%% 3) BATERIE LI-ION (EEC + ENERGIE)
densitate_energie_bat = 240;    % [Wh/kg]
V_nom_pack            = 22.2;   % [V]
eta_coulomb           = 0.995;  % [-]

% Parametri EEC (aleși pentru dinamica vizibilă)
R0_ref   = 0.18;      % [ohm]
R1_ref   = 0.08;      % [ohm]
C1_ref   = 1200;      % [F]
T_ref    = 298.15;    % [K]

k_soc_R0 = 0.50;      % [-] R0 creste la SOC mic
k_T_R0   = 0.025;     % [1/K] influenta T

% OCV(SOC) polinomial (didactic)
OCV_poly = [ -12.0, 25.0, -14.5, 4.8, 3.10 ]; % a4..a0
dUoc_dT  = -1.2e-3;   % [V/K] entropic

% Protectii
SOC_min_stop  = 0.20;    % 20%
V_min_stop    = 18.0;    % [V]
T_warn        = 313.15;  % 40C
T_crit_stop   = 333.15;  % 60C

```

Figure 4: Li-Ion Battery

The battery is modeled using a first-order equivalent electrical circuit (EEC), consisting of a SOC-dependent voltage source (OCV) and an RC branch that captures transient polarization. The energy density allows the conversion of battery mass into initial available energy:[18]

$$E_{\text{bat},0} = m_{\text{bat}} \cdot \rho_E \cdot 3600 [\text{J}]$$

Where:

- ρ_E is the energy density in [Wh/kg].

The OCV function is approximated polynomially as a function of SOC, and the term dU_{oc}/dT introduces an entropic thermal correction, also used in the thermal balance. The ohmic resistance $R_0$is formulated to increase at low SOC and to be temperature-dependent, reflecting trends observed in Li-Ion batteries.

5.5. Capacitor Parameterization and Energy–Voltage Conversion

```
%% 4) SUPERCAPACITOR (parametri pentru variatii vizibile)
E_sc_nom    = 12*3600;   % [J] ~12 Wh
masa_sc     = 0.25;      % [kg]
eta_sc      = 0.98;

Vsc_max     = 24;        % [V]
Vsc_min     = 14;        % [V]
C_sc        = 2*E_sc_nom/(Vsc_max^2); % [F]
Rsc         = 0.05;      % [ohm]
Psc_max     = 700;       % [W]
```

Figure 5: Parameters for Visible Variations

The capacitor is introduced as a high-power-density element, used to cover transient power demands. The fundamental relationship applied in the model is:[19]

$$E_{sc} = \frac{1}{2} C_{sc} V_{sc}^2 \Rightarrow V_{sc} = \sqrt{\frac{2E_{sc}}{C_{sc}}}$$

The capacitance $C_{sc}$is determined from the nominal energy and maximum voltage, ensuring dimensional consistency and allowing the voltage to be calculated at each integration step. The limitations $V_{sc,min}$and $P_{sc,max}$ impose realistic technological constraints (operation is not allowed below a minimum voltage, and power is saturated at a maximum).

5.6. Parameters of the Lumped Thermal Model

```
%% 5) MODEL TERMIC (lumped) - setat sa genereze derating vizibil
Cp_th       = 750;       % [J/kg/K]
A_surf      = 0.015;     % [m^2]
L_char      = 0.08;      % [m]
T_amb       = 293.15;    % [K] 20C
```

Figure 6: Thermal Model

The thermal model is formulated using a lumped-parameter differential equation, suitable for situations where the internal temperature distribution can be approximated as uniform (low Biot number). The temperature evolution is governed by the energy balance:[18], [19]

$$mC_p \frac{dT}{dt} = q_{gen} - hA(T - T_{amb})$$

Where:

- q_{gen} represents the internally generated heat;
- A_{surf} is the surface area;
- L_{char} is the characteristic length, which directly influences cooling;
- T_{amb} defines the thermal boundary condition.

5.7. *Profile definition and time discretization*

```
%% 6) PROFIL DE ZBOR
t_decolare  = 60;
t_stationar = 900;
t_deplasare = 600;
t_aterizare = 60;

dt      = 1;
t_total = t_decolare + t_stationar + t_deplasare + t_aterizare;
t       = (0:dt:t_total)';

```

Figure 7: Flight Profile

The mission is modeled as a sequence of phases with predefined durations (takeoff, hover, cruise, landing). Temporal discretization uses a time step dt, and the time vector is obtained by uniformly sampling the total interval. This formulation allows straightforward implementation of discrete updates for SOC, energy, and temperature through explicit numerical integration (Euler method).

5.8. *Regime parameterization: speed and power multipliers*

```
% viteze aer (m/s)
v_hover   = 4;
v_cruise  = 15;
v_landing = 3;

% multiplicatori de putere pe faze
kP_takeoff = 1.70;
kP_hover   = 1.00;
kP_cruise  = 1.25;
kP_landing = 0.80;

```

Figure 8: Flight Parameters

This block defines the aerodynamic regime for each flight phase through the effective airspeed and power multiplier factors. The use of power multipliers $k_P$allows representation of differences in mechanical load without introducing a full thrust control model. Specifically, takeoff is penalized energetically (factor > 1), while landing is associated with relatively lower power consumption.

5.9. *Modeling of power demand: induced, aerodynamic drag, and fixed loads*

```
%% 7) FUNCTII DE PUTERE
P_indus_hover = @(m) ((m*g)^(3/2)) / sqrt(2*rho_air*A_disk) / eta_motor;
P_drag        = @(v) 0.5*rho_air*CdA*v^3;

P_total_phase = @(m,kP,v) ...
    (P_indus_hover(m)*kP + P_drag(v)) + P_electronica + P_senzori;

```

Figure 9: Flight Functions

The total power is constructed additively from three main components: induced power (lift), power associated with aerodynamic drag during forward flight, and constant electrical loads.

The induced power is a nonlinear function of mass, expressed as:[6], [19]

$$P_{\text{ind}} \propto \frac{(mg)^{\frac{3}{2}}}{\sqrt{2\rho A}}$$

While the aerodynamic drag term follows a cubic dependence on velocity:

$$P_{\text{drag}} = \frac{1}{2}\rho\, C_d A\, v^3$$

This structure captures the essential characteristic of UAVs: flight autonomy is simultaneously influenced by vehicle mass and the kinematic regime.

5.10. Initial simulation run and extraction of key indicators

```
%% 8) SIMULARE INITIALA (fara optimizare)
masa_bat_initial = 0.65;

rez0 = simulare_misiune_extinsa( ...
    masa_bat_initial, masa_structura, masa_sc, masa_maxima, ...
    densitate_energie_bat, V_nom_pack, ...
    R0_ref,R1_ref,C1_ref,T_ref,k_soc_R0,k_T_R0, ...
    OCV_poly,dUoc_dT,eta_coulomb, ...
    E_sc_nom,C_sc,Vsc_max,Vsc_min,Rsc,Psc_max,eta_sc, ...
    Cp_th,A_surf,L_char,k_air,nu_air,Pr_air,T_amb, ...
    SOC_min_stop,V_min_stop,T_warn,T_crit_stop, ...
    t,dt, ...
    t_decolare,t_stationar,t_deplasare,t_aterizare, ...
    kP_takeoff,kP_hover,kP_cruise,kP_landing, ...
    v_hover,v_cruise,v_landing, ...
    P_total_phase);

fprintf('\n=== SIMULARE INITIALA ===\n');
fprintf('Masa baterie: %.2f kg\n', masa_bat_initial);
fprintf('Autonomie: %.2f minute\n', rez0.timp_zbor/60);
fprintf('Motiv oprire: %s\n', rez0.motiv_stop);
fprintf('SOC final baterie: %.1f %%\n', 100*rez0.SOC_bat(rez0.idx_stop));
fprintf('Tmax baterie: %.1f C\n', rez0.Tmax_C);
fprintf('E_total: %.1f Wh | E_bat: %.1f Wh | E_sc: %.1f Wh\n', rez0.E_total_Wh, rez0.E_bat_Wh, rez0.E_sc_Wh);
fprintf('Loss_bat: %.1f Wh | Loss_sc: %.1f Wh\n', rez0.E_loss_bat_Wh, rez0.E_loss_sc_Wh);
```

Figure 10: Initial Simulation

The initial simulation represents the reference scenario. Results are summarized through: the effective flight time (autonomy), the reason for termination (minimum SOC, minimum voltage, critical temperature, or end of mission), and state parameters at the stop time. This step is necessary to provide a baseline for comparison when the optimization procedure is applied.

5.11. Battery mass optimization using fmincon

```
%% 9) OPTIMIZARE MASA BATERIE (maximizare autonomie)
lb = 0.50;
ub = masa_maxima - masa_structura - masa_sc;

options = optimoptions('fmincon', ...
    'Display','iter', ...
    'Algorithm','sqp', ...
    'MaxFunctionEvaluations', 250);

[masa_bat_opt, fval] = fmincon( ...
    @(m) obiectiv_autonomie_ext(m, masa_structura, masa_sc, masa_maxima, ...
        densitate_energie_bat, V_nom_pack, ...
        R0_ref,R1_ref,C1_ref,T_ref,k_soc_R0,k_T_R0, ...
        OCV_poly,dUoc_dT,eta_coulomb, ...
        E_sc_nom,C_sc,Vsc_max,Vsc_min,Rsc,Psc_max,eta_sc, ...
        Cp_th,A_surf,L_char,k_air,nu_air,Pr_air,T_amb, ...
        SOC_min_stop,V_min_stop,T_warn,T_crit_stop, ...
        t,dt, ...
        t_decolare,t_stationar,t_deplasare,t_aterizare, ...
        kP_takeoff,kP_hover,kP_cruise,kP_landing, ...
        v_hover,v_cruise,v_landing, ...
        P_total_phase), ...
    masa_bat_initial, [],[],[],[], lb, ub, [], options);

rez_opt = simulare_misiune_extinsa( ...
    masa_bat_opt, masa_structura, masa_sc, masa_maxima, ...
    densitate_energie_bat, V_nom_pack, ...
    R0_ref,R1_ref,C1_ref,T_ref,k_soc_R0,k_T_R0, ...
    OCV_poly,dUoc_dT,eta_coulomb, ...
    E_sc_nom,C_sc,Vsc_max,Vsc_min,Rsc,Psc_max,eta_sc, ...
    Cp_th,A_surf,L_char,k_air,nu_air,Pr_air,T_amb, ...
    SOC_min_stop,V_min_stop,T_warn,T_crit_stop, ...
    t,dt, ...
    t_decolare,t_stationar,t_deplasare,t_aterizare, ...
    kP_takeoff,kP_hover,kP_cruise,kP_landing, ...
    v_hover,v_cruise,v_landing, ...
    P_total_phase);

fprintf('\n=== OPTIMIZARE ===\n');
fprintf('Masa baterie optima: %.3f kg\n', masa_bat_opt);
fprintf('Autonomie optimizata: %.2f minute\n', rez_opt.timp_zbor/60);
fprintf('Motiv oprire: %s\n', rez_opt.motiv_stop);
fprintf('Tmax baterie: %.1f C\n', rez_opt.Tmax_C);
fprintf('Derating mediu: %.2f\n', mean(rez_opt.derating_factor(1:rez_opt.idx_stop)));
fprintf('E_total: %.1f Wh\n', rez_opt.E_total_Wh);
```

Figure 11: Battery Mass Optimization

The problem is formulated as a nonlinear constrained optimization:

$$max_{mbat} t_{\mathrm{flight}}(m_{\mathrm{bat}}), m_{\mathrm{bat}} \in [lb, ub]$$

The SQP (Sequential Quadratic Programming) method is suitable because it efficiently handles nonlinear problems with simple constraints, and the objective function is evaluated by running the complete simulation for each candidate battery mass m_{bat}.

In this way, the optimization implicitly incorporates the nonlinear effects of mass on energy consumption and of current on temperature and voltage.

5.12. *Graph generation for results interpretation*

Figure 12: Graph Generation 1

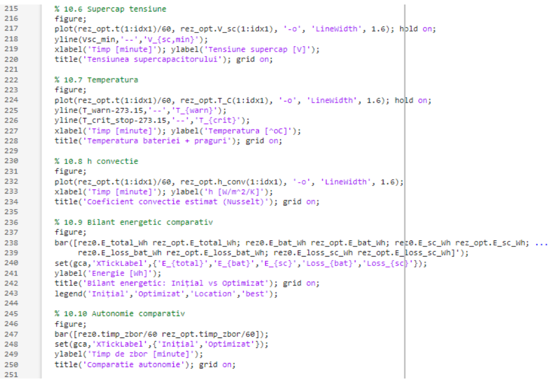

Figure 13: Graph Generation 2

The graphs are used to transform numerical outputs into interpretable information. For the state of charge, there is an interaction between the battery that provides the necessary energy and the supercapacitor that takes the peaks for optimal operation. The introduction of markers ("-o") also has a practical role: it ensures the visibility of the curves even in scenarios where the simulation stops prematurely due to a constraint.

5.13. *Objective Function*

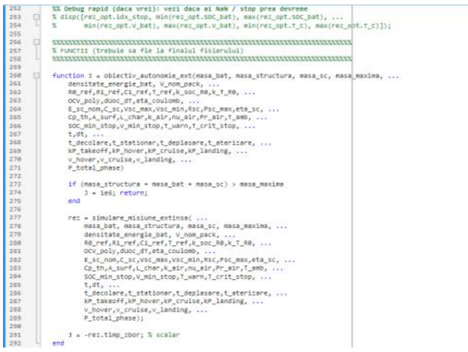

Figure 14: Maximizing Flight Autonomy

The objective function is formulated so that maximizing flight autonomy is converted into a minimization problem compatible with fmincon. This conversion is performed as follows:[20]

$$J(m_{\text{bat}}) = -t_{\text{flight}}(m_{\text{bat}})$$

In this way, the optimal solution corresponds to the battery mass that produces the longest flight time before reaching any operational limit.

5.14. *Main simulation function: complete energy chain*

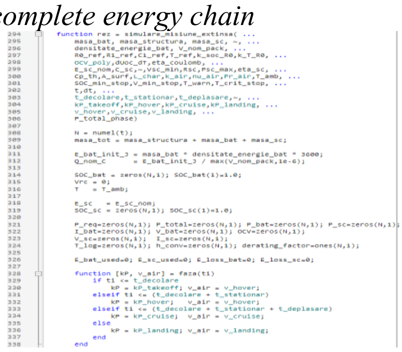

Figure 15: Simulation Function

The simulation function performs, at each time step, a consistent calculation of energy flows and state variables. In terms of modeling architecture, it can be interpreted as a “numerical observer” that propagates SOC, voltage, and temperature based on the power demand imposed by the flight profile.

Key elements include:

- Derivation of current from the power demand and the EEC model;
- Application of protections as conditional stops;
- Closure of the electro-thermal loop (current → losses → temperature → derating).

6. Interpretation of Graphs Obtained from the Simulation

The results obtained based on the simulation, aiming to evaluate the performance of the storage system in MATLAB for research drones. [21]. Based on the developed electro-thermal model, a series of graphs were obtained to highlight the main parameters of the system for different regimes in which it is used. Leveraging the electro-thermal framework established in the preceding sections, several datasets were visualized to demonstrate the dynamic response of the power system's core parameters across diverse operational envelopes.[5], [22]

The resulting graphical analysis facilitates a rigorous evaluation of the discharge profiles for both the standalone lithium-ion configuration and the hybrid battery-supercapacitor topology. By examining these trends, it becomes possible to isolate the specific impacts of current fluctuations, voltage drops, and power demands on the system's thermal evolution and net efficiency. These observations are instrumental in diagnosing how transient loads influence the long-term reliability and performance of the integrated energy architecture. The simulation results provide insight into how energy management strategies and component sizing influence the operational stability and energy efficiency of the UAV platform. The advantages of using the optimized storage system are observed, as well as reducing the demands on the battery to improve voltage stability and achieve a longer flight duration.

6.1. State of charge (SOC) evolution

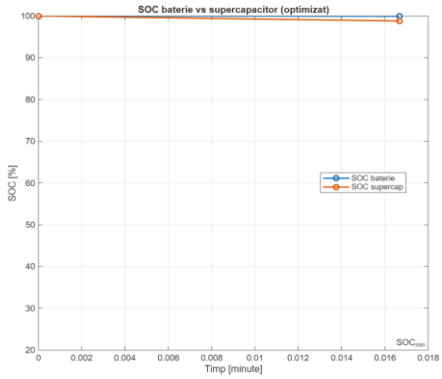

Figure 16: Battery and Capacitor

Figure 16 shows the charge fluctuations on the two sources, i.e. the Li-Ion battery and the supercapacitor. In parallel, the capacitor’s charge state changes in a more abrupt and temporally localized manner. This is due to the fact that it is not used constantly. We observe faster discharge followed by periods in which the supercapacitor’s energy is constant.[23] In an engineering interpretation, this figure confirms the role of the capacitor as an energy “buffer” element, which reduces the dynamic demands on the battery and implicitly the amplitude of the peak currents.

In parallel, the supercapacitor SOC changes in a more abrupt and temporally localized manner. This behavior is a consequence of its primary use in transient conditions, when the power demand exceeds a predefined threshold. Episodes of faster discharge correspond to power “bursts,” followed by periods where the capacitor energy remains relatively constant (since the model does not include an explicit recharging phase from the battery).[24] From an engineering perspective, this figure confirms the role of the supercapacitor as an energy "buffer," which reduces dynamic stress on the battery and, consequently, the amplitude of peak currents.

6.2. Requested power vs. supplied power and load sharing

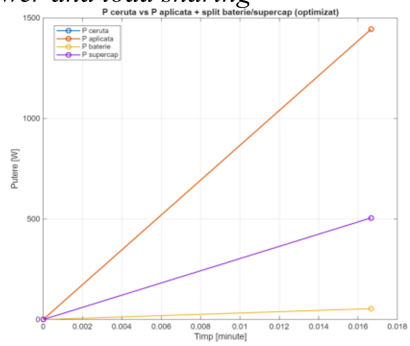

Figure 17: Requested Power and Supplied Power

Figure 17 shows the comparison between the power required by the use of the drone and how the battery and supercapacitor are used according to the requirements. The P_{req}curve represents the energy requirement derived from the aerodynamic model (induced power and drag power), complemented by auxiliary consumption from electronics and sensors. The presence of periodic bursts induces rapid variations in the requested power, simulating realistic demand scenarios (maneuvers, position corrections, wind gusts, or changes in propulsion regime).[25]

The $P_{\mathrm{bat}}$and P_{sc}curves represent the power allocation strategy. During intervals where the power demand exceeds the activation threshold, the supercapacitor supplies a fraction of the requirement, observed as an increase in P_{sc}accompanied by a relative reduction in P_{bat}.

From an energy perspective, this redistribution mitigates stress on the battery during high-power phases, reducing ohmic losses (proportional to I^2R) and helping maintain voltage within functional limits. Therefore, this figure validates the "power split" logic and highlights the advantage of the hybrid architecture during transient regimes.[26]

6.3. Thermal derating factor

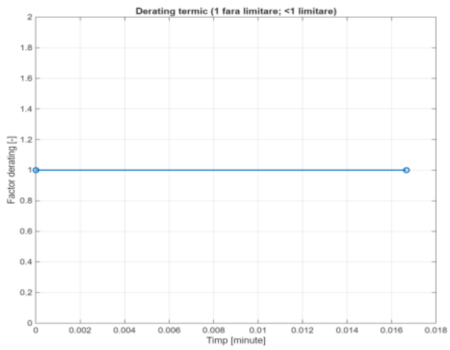

Figure 18: Power Limitation Based on Temperature

Figure 18 illustrates the evolution of the thermal derating factor, defined as a dimensionless coefficient $\alpha \in (0,1]$ which modulates the available power depending on the temperature of the storage system. We can observe values close to 1 indicating operation without thermal restrictions.

The interpretation of this graph is directly related to operational safety: when the temperature exceeds the warning threshold T_{warn}, the model gradually reduces the applied power, which implicitly limits current and, consequently, reduces internal heat generation. From an energy management perspective, this figure demonstrates that flight autonomy is not determined solely by available energy, but also by thermal constraints that may impose performance reductions before the SOC is fully depleted.

6.4. Battery terminal voltage and minimum allowed threshold

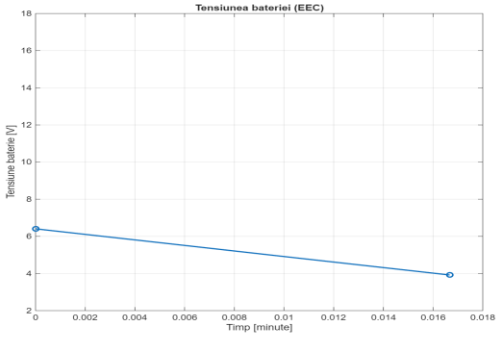

Figure 18: Battery Voltage

Figure 18 shows the voltage at the battery terminals during transmission, as well as the minimum threshold $V_{\min}$ for the protection limit. The voltage is achieved by combining the open circuit voltage, voltage drops R_0, and the polarization voltage V_{RC}. [24], [25]Consequently, the terminal voltage is not only an indicator of the remaining energy but also a parameter sensitive to current demands.

Steeper voltage drops typically occur during high-power intervals, when current increases and the ohmic drop becomes dominant. Maintaining the voltage above the minimum threshold is essential to prevent deep discharge and ensure the stability of UAV subsystems. Therefore, this figure highlights the critical relationship between power demand and the electrical feasibility of the mission, emphasizing that operational limitation can be imposed by voltage even before the SOC reaches its minimum threshold.

6.5. Battery current and transient nature of the load

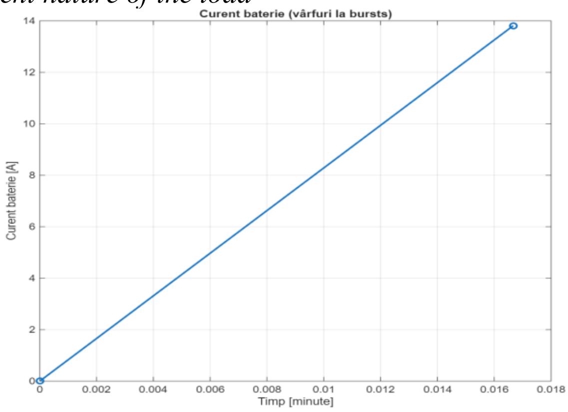

Figure 19: Battery current

In figure 19 we find the current supplied by the battery and calculated from the power requirement and the EEC model. The significance of this graph lies in the fact that the current magnitude simultaneously determines: (i) Joule losses, (ii) internal heating, (iii) voltage drop, and (iv) the rate of charge consumption (Coulomb Counting).[27], [28]

Current peaks are observed during periods of high-power demand or when the supercapacitor cannot fully absorb the load due to its own limits (minimum voltage or available energy). An effective hybridization strategy should reduce the amplitude of these peaks to minimize electrochemical stress on the battery.

Therefore, this figure is relevant not only for flight autonomy but also for durability, as high-current regimes accelerate degradation processes and increase thermal risk.

6.6. Supercapacitor voltage and minimum operating threshold

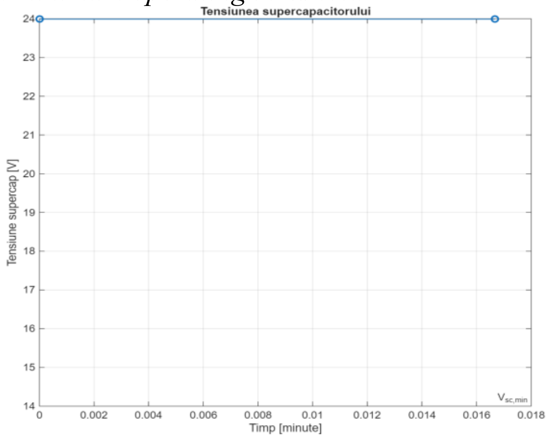

Figure 20: Supercapacitor Voltage

Figure 20 shows the supercapacitor voltage, a nonlinear variable with respect to the stored energy, according to the relationship $E = \frac{1}{2}CV^2$. Compared to the battery, the supercapacitor has a faster voltage variation, while the energy is consumed quickly.[29]

Considering the hybrid architecture, the real availability of the supercapacitor as a power source, and if the voltage drops below the threshold, this means either that the nominal energy is insufficient for the profile or the use of the drone is too demanding for the battery. Conversely, if the voltage remains high, the supercapacitor is under-utilized and could be resized (mass/volume optimization).

6.7. Battery temperature and warning/critical thresholds

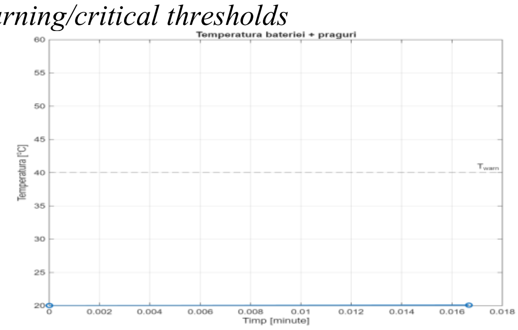

Figure 21: Battery Temperature

Figure 21 highlights the evolution of the battery temperature along with the warning (T_{warn}) and critical (T_{crit}) thresholds. The temperature results from an energy balance between internally generated heat (dominated by Joule losses and polarization effects) and convective dissipation to the ambient environment. This figure is fundamental for safety analysis, as exceeding the critical threshold triggers the simulation stop (thermal protection).

Temperature rises are correlated with current peaks and high-power periods, validating the consistency of the electro-thermal model. Additionally, during intervals when thermal derating is active, the temperature slope tends to decrease because the applied power is limited and internal heat generation is reduced. Thus, the figure demonstrates the role of derating as a preventive control mechanism, with a direct impact on maintaining thermal integrity.

6.8. Convective heat transfer coefficient $h(t)$estimated via Nusselt correlations

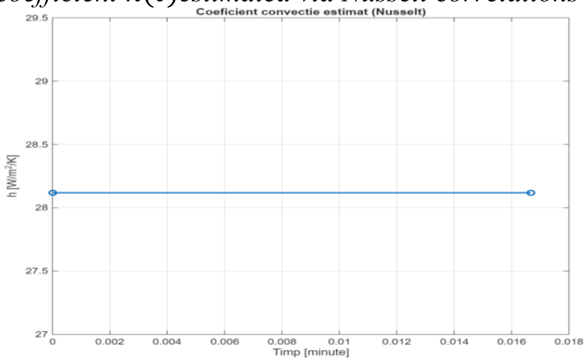

Figure 22: Convection Coefficient

The dynamics of the convective heat transfer coefficient, h, are illustrated in Figure 22, where the values are derived from local airflow velocity and the thermophysical characteristics of the ambient environment. To accurately quantify this interaction, the model implements a forced convection correlation defined by the relationship:[30]

$$Nu = 0.664\, Re^{\frac{1}{2}} Pr^{\frac{1}{3}}, h = \frac{k_{\mathrm{air}}}{L} Nu$$

As a result, transitions between distinct operational envelopes—such as the shift from hovering to forward cruise—trigger fluctuations in airspeed that directly modulate the magnitude of h. The underlying physics indicate that increased velocities catalyze the heat transfer rate, thereby enhancing the platform's thermal dissipation capacity and preventing heat accumulation within the power electronics.

This graph explains why the same electrical load can produce different thermal responses depending on the flight regime, emphasizing the necessity of integrating aerodynamic terms into the thermal model for accurate simulation of UAV energy storage systems.

6.9. Comparative energy balance: initial vs. optimized configuration

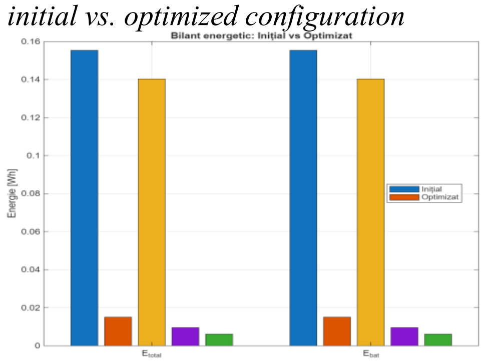

Figure 22: Energy Balance

Figure 22 provides an energy summary for the two scenarios: the initial configuration and the optimized configuration. Total energy consumption, energy delivered by the battery, energy supplied by the supercapacitor, and losses associated with each subsystem are compared.[20], [31] This aggregated representation offers an "energy audit" perspective, useful for evaluating overall system efficiency.

6.10. Comparison of flight autonomy (mission duration) for the analyzed scenarios

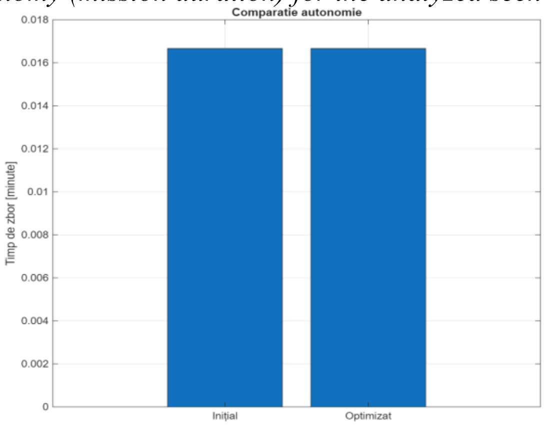

Figure 23: Autonomy Comparison

Figura 23 prezintă comparația dintre autonomia din cazul inițial și cazul optimizat, prin durata efectivă a misiunii.[13], [32], [33]

7. Conclusion

This paper analyzed the efficiency of energy storage systems for marine drones. A model was developed for the batteries.[9], [33] Li-Ion, made using equivalent circuits, this method providing a good energy efficiency for the energy consul needed during flights.

The data obtained during the simulation were entered into the MATLAB platform showing the advantages of the hybrid configuration.[34], [35] The integration of the supercapacitor facilitates the handling of sudden loads and power peaks, reducing the intensity of the currents passing through the battery. The numerical interpretation showed a balance between the storage capacity of the battery and the total weight of the drone. If we have a larger battery, it also results in a larger energy reserve, from this point of view the batteries have been resized to have an ideal mass with a good energy efficiency.[36], [37]

In addition, this paper shows the thermal limitations that a hybrid system may have.[37], [38]. From here we can see that sudden changes in the flight regime affect the thermal variations that lead to the degradation of the drone's energy system, so the implementation of a thermal management system becomes essential to have the highest possible efficiency.[37], [38]

In conclusion, the paper validates the importance of numerical modeling and simulation methods as effective means for the development and optimization of energy architectures for UAV systems. The proposed methodology allows for the assessment of the impact of energy, thermal, and aerodynamic parameters on flight autonomy and provides an analytical framework for the optimal sizing of energy storage systems.

For future research directions, it is proposed to extend the model by including advanced battery state estimation algorithms and to validate the simulation results experimentally, with the aim of improving model accuracy and applicability to real UAV systems.

References

1. Y. Han and W. Ma, "Automatic monitoring of water pollution based on the combination of UAV and USV," in 2021 IEEE 4th International Conference on Electronic Information and Communication Technology, ICEICT 2021, Institute of Electrical and Electronics Engineers Inc., Aug. 2021, pp. 420–424. doi: 10.1109/ICEICT53123.2021.9531204.
2. Q. Cai and Y. Han, "A Navigation Control Evaluation Method of USV Based on Fuzzy Rough Set," in CTISC 2022 - 2022 4th International Conference on Advances in Computer

Technology, Information Science and Communications, Institute of Electrical and Electronics Engineers Inc., 2022. doi: 10.1109/CTISC54888.2022.9849738.

3. Q. Cai and Y. Han, “A Navigation Control Evaluation Method of USV Based on Fuzzy Rough Set,” in CTISC 2022 - 2022 4th International Conference on Advances in Computer Technology, Information Science and Communications, Institute of Electrical and Electronics Engineers Inc., 2022. doi: 10.1109/CTISC54888.2022.9849738.
4. F. M. Raimondi, M. Trapanese, V. Franzitta, A. Viola, and A. Colucci, “A innovative semi-immergible USV (SI-USV) drone for marine and lakes operations with instrumental telemetry and acoustic data acquisition capability,” in MTS/IEEE OCEANS 2015 - Genova: Discovering Sustainable Ocean Energy for a New World, Institute of Electrical and Electronics Engineers Inc., Sep. 2015. doi: 10.1109/OCEANS-Genova.2015.7271595.
5. M. Boxwell, “Solar Electricity Handbook A simple, practical guide to solar energy: how to design and install photovoltaic solar electric systems.” [Online]. Available: www.GreenstreamPublishing.com
6. K. Sabeel, G. Aggarwal, M. Eslamy, Rani, R. Kumar, and A. Paramel, “Impact of Charging Speed on Electric Vehicle Battery Life,” 2024 11th International Conference on Electrical and Electronics Engineering, ICEEE 2024, pp. 254–259, 2024, doi: 10.1109/ICEEE62185.2024.10779302.
7. IEEE Staff, 2011 International Conference on Electric Information and Control Engineering. IEEE, 2011.
8. S. Li et al., “An Optimization Model for Joint Participation of Wind, Photovoltaic and Storage in the Day-ahead Electricity Spot Market Considering Output Uncertainty,” in 2024 IEEE 8th Conference on Energy Internet and Energy System Integration, EI2 2024, Institute of Electrical and Electronics Engineers Inc., 2024, pp. 2316–2322. doi: 10.1109/EI264398.2024.10991566.
9. “Basic Electrical Engineering (PDFDrive)”.
10. H. L. Hibbard, W. ’ Hetherington, A. I. E. E. Fellow, and A. I. E. E. Associate, “Historical Review of Electrical Applications on Shipboard.”
11. V. Kandasamy and M. Venkatesan, “Adaptive Electric Vehicle Charging Method to Improve the Battery Life,” 2nd International Conference on Advancements in Electrical, Electronics, Communication, Computing and Automation, ICAECA 2023, pp. 1–4, 2023, doi: 10.1109/ICAECA56562.2023.10200210.
12. V. Pop, H. Jan Bergveld, D. Danilov, P. P. Regtien, and P. H. Notten, “Battery Management Systems: Accurate State-of-Charge Indication for Battery-Powered Applications (Philips Research Book Series).”
13. B. Reeves, “Solar Power DIY Handbook. So, You Want To Connect Your Off-Grid Solar Panel to a 12 Volts Battery?”
14. M. O. Qays, Y. Buswig, M. L. Hossain, and A. Abu-Siada, “Recent progress and future trends on the state of charge estimation methods to improve battery-storage efficiency: A review,” CSEE Journal of Power and Energy Systems, vol. 8, no. 1, pp. 105–114, 2022, doi: 10.17775/CSEEJPES.2019.03060.
15. Y. Zhang, “Modularized Battery Management Systems for Lithium-Ion Battery Packs in EVs.”
16. L. Zhijie and Z. Wei, “Power battery charging device design,” ITOEC 2023 - IEEE 7th Information Technology and Mechatronics Engineering Conference, vol. 7, pp. 1365–1370, 2023, doi: 10.1109/ITOEC57671.2023.10292109.
17. K. V. Raj, K. Rayudu, and G. Battapothula, “Critical Review on Battery Management Systems,” Proceedings - International Conference on Applied Artificial Intelligence and Computing, ICAAIC 2022, no. Icaaic, pp. 1676–1680, 2022, doi: 10.1109/ICAAIC53929.2022.9793001.
18. B. Images, “The Handbook of Lithium-Ion Battery Pack Design.”
19. M. Haqqi, Z. Benmamoun, H. Hachimi, Y. Raouf, I. Jebbor, and M. Akikiz, “Renewable and Sustainable Energy: Solar Energy and Electrical System Design,” in 2023 9th International

Conference on Optimization and Applications, ICOA 2023 - Proceedings, Institute of Electrical and Electronics Engineers Inc., 2023. doi: 10.1109/ICOA58279.2023.10308842.
20. Y. Zhang, Z. Qiang, W. Ningbo, G. Pengfei, D. Kun, and Z. Zhang, "The Key Technology of the Coordinated Control System of Wind Power and Energy-intensive Load."
21. J. Zhang, R. Sun, Y. Long, R. Bo, and J. Liu, "A Review of Energy Storage: Economic Viability, Social Impacts, and Future Directions," in Proceedings of the IEEE International Conference on Service Operations and Logistics, and Informatics, SOLI, Institute of Electrical and Electronics Engineers Inc., 2024. doi: 10.1109/SOLI63266.2024.10956045.
22. R. Ranjith Kumar, C. Bharatiraja, K. Udhayakumar, S. Devakirubakaran, K. S. Sekar, and L. Mihet-Popa, "Advances in Batteries, Battery Modeling, Battery Management System, Battery Thermal Management, SOC, SOH, and Charge/Discharge Characteristics in EV Applications," IEEE Access, vol. 11, no. September, pp. 105761–105809, 2023, doi: 10.1109/ACCESS.2023.3318121.
23. X. Chen, Association of Global Intelligent Science and Technology, and M. IEEE Systems, Proceedings of the International Conference on Cyber-Physical Social Intelligence (ICCSI 2022) Nanjing, China, November 18-21, 2022.
24. L. Technology Standards Committee of the IEEE Computer Society, "IEEE Standard for Learning Technology-Extensible Markup Language (XML) Schema Binding for Data Model for Content Object Communication IEEE Computer Society Sponsored by the Learning Technology Standards Committee," 2004.
25. L. Technology Standards Committee of the IEEE Computer Society, "IEEE Standard for Learning Technology-Extensible Markup Language (XML) Schema Binding for Data Model for Content Object Communication IEEE Computer Society Sponsored by the Learning Technology Standards Committee," 2004.
26. IEEE Electrical Insulation Society Staff, 2012 12th International Conference on Control Automation Robotics and Vision.
27. F. Zhang, "CU Scholar Modeling and Control of a Modular Battery Management System for Lithium-ion Battery Packs." [Online]. Available: https://scholar.colorado.edu/ecen_gradetdshttps://scholar.colorado.edu/ecen_gradetds/153
28. "A Systems Approach to Lithium-Ion Battery Management."
29. K. R. Ahmad, P. J. Grbovic, G. De Falco, and R. Petrella, "Li-Ion Battery Fast Charging Methods: Review and Comparison," 2024 IEEE 10th International Power Electronics and Motion Control Conference, IPEMC 2024 ECCE Asia, no. Cccv, pp. 5131–5137, 2024, doi: 10.1109/IPEMC-ECCEAsia60879.2024.10567271.
30. M. Sesharanjith, M. Vishaal Dharsan, G. Sundaresh, K. Darshan, and S. Arunkumar, "Li- Ion Battery Life Cycle Estimation by KNN Algorithm," 8th International Conference on Electronics, Communication and Aerospace Technology, ICECA 2024 - Proceedings, no. Iceca, pp. 683–686, 2024, doi: 10.1109/ICECA63461.2024.10800892.
31. J. Miguel and B. Marques, "magem Battery Management System (BMS) for Lithium-Ion Batteries Master Dissertation," 2014.